Single Molecule Study of Xanthan Conformation Using Atomic Force Microscopy

ARTICLE *in* BIOMACROMOLECULES · FEBRUARY 2001

Impact Factor: 5.75 · DOI: 10.1021/bm015555g · Source: PubMed

2 AUTHORS:

Terri A Camesano
Worcester Polytechnic Institute
93 PUBLICATIONS **2,400** CITATIONS
SEE PROFILE

Kevin J Wilkinson
Université de Montréal
162 PUBLICATIONS **5,075** CITATIONS
SEE PROFILE

Single Molecule Study of Xanthan Conformation Using Atomic Force Microscopy

Terri A. Camesano*,† and Kevin J. Wilkinson‡

Department of Chemical Engineering, Worcester Polytechnic Institute, 100 Institute Road, Worcester, Massachusetts 01609; and CABE (Analytical and Biophysical Environmental Chemistry), University of Geneva, 30 Quai Ernest Ansermet, CH-1211 Geneva 4, Switzerland

Received May 1, 2001; Revised Manuscript Received August 9, 2001

Conformations of individual macromolecules of the biopolymer xanthan were investigated using atomic force microscopy (AFM). Xanthan from very dilute solutions (1 ppm) was allowed to adsorb onto freshly cleaved mica and examined using tapping mode AFM under ambient conditions. The secondary structure of xanthan was probed by heating the polymer and gradually cooling, which denatured and renatured the polymer. When salt was present, renatured xanthan formed a double helical structure, consistent with the structure of native xanthan. In pure water, renaturation was not complete as what appeared to be single helical structures were observed. The number-average contour length (L_n) of the polymer in its single helical state was 1651 nm. In the double helical state, induced by the addition of salt, L_n decreased to 450 nm (in 0.5 M KCl). The chains also became less rigid as salt was added. The persistence length decreased from 417 nm in pure water to ∼150 nm in 0.1 or 0.5 M KCl. This indicated a trend toward more flexible molecules when salt was present. Calculations of end-to-end distances based on equilibrium and projected conformations confirmed that the xanthan chain conformation on the mica surface was at equilibrium and was therefore representative of the conformation of xanthan in solution. The single-molecule AFM technique eliminates one common bias of solution techniques, which is the determination of an average signal between aggregates and dissolved molecules. It is thus a useful complement to solution-based methods for determining physical−chemical properties of biopolymers.

Introduction

One motivating factor behind studies of the conformations of bacterial polysaccharides stems from the role these polymers play in adhesion and coagulation in natural systems. For example, bacterial adhesion to surfaces such as soil, water distribution systems, devices that can be implanted into the body, teeth, contact lenses, etc. is hypothesized to be controlled by the physical−chemical properties of surface polymers.[1,2] Polysaccharides are also implicated in the binding of metals and the coagulation of clay and other colloids in natural aquatic systems.[3,4] In this study, xanthan, produced by *Xanthomonas campestris*[5,6] was chosen as a model biopolymer because it has a negative charge and a size similar to many other polysaccharides of interest in environmental and biomedical engineering. Known commercially as xanthan gum, it is also important in many industrial applications because it exhibits high viscosities in aqueous solutions over a wide range of salt concentrations and pH.[6] It is used as an emulsifier in the food industry and was used extensively in enhanced oil recovery.[7]

Properties of biopolymers that govern behavior include size, shape, flexibility, charge, and the presence of specific functional groups. The range of conformations possible in polysaccharides and the principles governing intramolecular interactions are less well understood than for other macromolecules, such as polynucleotides and proteins. This poor understanding stems in part from the limitations of available analytical techniques, and in part due to the complex behavior of biopolymers. Numerous solution techniques have been employed for studying the conformation of xanthan, including optical rotation,[6,8] circular dichroism,[9−11] light scattering,[11−15] calorimetry,[16] viscosity or viscoelastic measurements,[6,11,17,18] electric birefringence,[19] neutron scattering,[10] NMR,[9,20] and size exclusion chromatography.[11] These studies, however, have sometimes produced conflicting results regarding xanthan's secondary structure. Polysaccharides often form aggregates in solution that can mask the behavior of individual macromolecules. A difficulty in establishing polysaccharide conformation is encountered in that solution techniques yield an average response based on a large number of molecules and aggregates. Additionally, because properties are measured on a bulk solution, it is possible to miss characteristics of smaller subpopulations that deviate from the average behavior.

AFM is an emerging technique that can help overcome some of the limitations of solution techniques by allowing for the direct imaging of individual macromolecules. Xanthan, along with other polysaccharides, has been imaged with AFM. Kirby et al.[21] were the first to demonstrate that xanthan

* Corresponding author. Telephone: 508-831-5380. Fax: 508-831-5853. E-mail: terric@wpi.edu.
† Worcester Polytechnic Institute.
‡ University of Geneva.

10.1021/bm015555g CCC: $20.00
Published on Web 09/20/2001

molecules could be imaged under 1-butanol using contact mode AFM. Their work was extended to include tapping mode imaging of xanthan under ambient conditions.[22] Capron et al.[23] imaged native and renatured xanthan in 2-propanol using contact mode AFM. Although a quantitative analysis was not performed, these studies showed that xanthan was fairly rigid. In addition, these early studies demonstrated that xanthan may form aggregated structures on mica under some conditions and warned of the need for adequate sample preparation.

Although images themselves are useful, quantitative calculations of polymer properties are needed to relate polymer structure to behavior. These relationships may be derived through analysis of individual macromolecules. Frontali et al.[24] developed techniques for quantifying DNA contour length and persistence length from SEM images. Their work demonstrated that if the passage from three dimensions to two dimensions is achieved under equilibrium conditions, the adsorption process preserves information regarding polymer stiffness. Through a statistical analysis of individual molecules, properties such as total contour length and persistence length can be calculated. Stokke et al.[25] applied the Frontali et al.[24] principles to calculate properties of xanthan from SEM images under a limited set of conditions.

The objective of our study is to provide quantitative conformational information for xanthan at four different salt concentrations by studying individual macromolecules. Atomic force microscopy and statistical image analysis were used to calculate biopolymer contour lengths, end-to-end distances, and persistence lengths. This information was used to explain the conformational changes xanthan undergoes as a function of salt concentration.

Materials and Methods

Xanthan was prepared similar to a method described previously.[21] Xanthan gum at a concentration of 1000 mg L^{-1} (Sigma) was stirred for 1−2 h while heating to 95 °C. The resulting solution was ultracentrifuged at 140000*g* for 3 h at 4 °C to remove large aggregates. The sample was diluted to 1 mg L^{-1} in either pure water or KCl of the desired concentration. A piece of freshly cleaved mica was placed into the solution and the polysaccharide was allowed to adsorb onto the mica. After 1 min, the mica was removed and dried in a Petri dish for 30−60 min.

Atomic force microscopy (Digital Instruments Nanoscopoe III Multimode) was performed under ambient conditions in tapping mode using TESP tips (Digital Instruments, spring constant = 2−100 nN/m, as reported by manufacturer). Images were collected of xanthan adsorbed from pure water, 0.01 M KCl, 0.1 M KCl, and 0.5 M KCl. For each condition, an analysis was made of 50 macromolecules. Images were digitized and processed as follows using the Fovea Pro 1.0 plug-ins for Adobe Photoshop. Each image was converted to gray scale and contrast enhanced before the threshold was set. After setting the threshold, a "close" filter was applied and the data were skeletonized, or converted to the width of one pixel. The pixelized data was opened in Sigma ScanPro 4.0, where the contour length and *x* and *y* coordinates of each data point in the chain were measured. From these raw data, the mean-square end-to-end distance and contour length were calculated.

The degree of polydispersity in the polymer sample was quantified as the ratio of the weight-average contour length (L_w) and number-average contour length (L_n), as

$$\text{polydispersity index} = \frac{L_w}{L_n} \tag{1}$$

where $L_n = \sum_n n_i L_i / \sum_n n_i$ and $L_w = \sum_n n_i L_i^2 / \sum_n n_i L_i$.

Chain Statistics. To make a quantitative analysis of chain flexibility, the persistence lengths were compared for the polymer under various chemical conditions. A statistical analysis of the change in tangent direction along the polymer contour length was calculated using techniques developed by Frontali et al.[24] The persistence length calculation is based on the following assumptions.

(1) The probability density function of the angle between consecutive links of the chain is Gaussian, and can be represented by

$$P(\theta(l)) = \left(\frac{L_p}{2\pi l}\right)^{1/2} \exp\left(-\frac{L_p \theta^2}{2l}\right) \tag{2}$$

where θ is the bend angle, l is the distance between segments, and L_p is the persistence length of the polymer.

(2) The observed two-dimensional conformation is obtained by permitted deformations, and is not a projection of the three-dimensional structure.

(3) The adsorbing surface does not alter the local rigidity of the polymer chain.

Frontali et al.[24] showed that the odd moments of the distribution (eq 2) are equal to zero, and for the even moments,

$$\langle \theta^2(l) \rangle = \frac{l}{L_p} \tag{3}$$

and

$$\langle \theta^4(l) \rangle / \langle \theta^2(l) \rangle^2 = 3 \tag{4}$$

The definition of the second moment (eq 3) was used to calculate L_p, while eq 4 was applied to check if the first assumption was valid.

To check assumptions two and three, a calculation was made to determine whether the polymer adopted an equilibrium conformation on the surface. For polymer chains that have reached equilibrium with the surface, their conformation will correspond to a 2D conformation rather than a 3D projection. The end-to-end distances corresponding to 2D and projected conformations are given by[26]

$$\langle R_{ee} \rangle_{2D}^2 = 4 L_p L \left(1 - \frac{2L_p}{L}(1 - e^{-L/2L_p})\right) \tag{5}$$

and

$$\langle R_{ee} \rangle_{proj}^2 = \frac{4}{3} L_p L \left(1 - \frac{L_p}{L}(1 - e^{-L/L_p})\right) \tag{6}$$

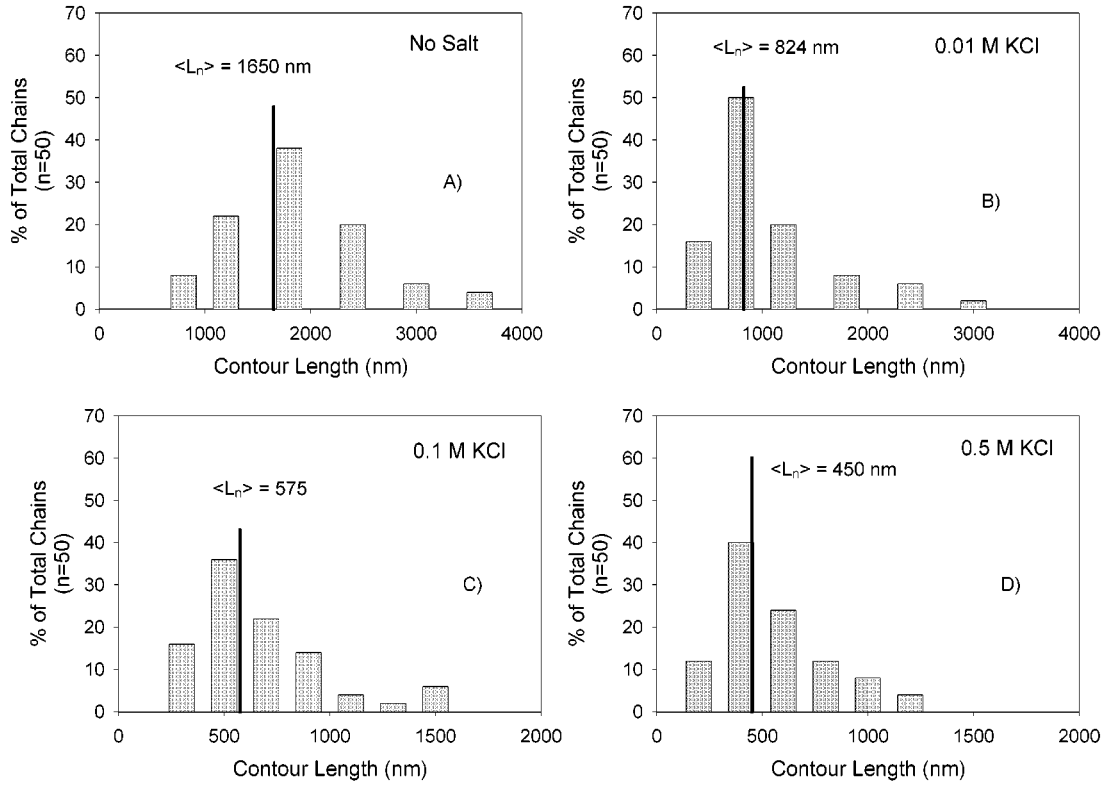

Figure 1. Distribution of contour lengths for xanthan chains in (A) pure water, (B) 0.01 M KCl, (C) 0.1 M KCl, and (D) 0.5 M KCl. In each case, the length was measured on 50 xanthan chains.

Table 1. Contour Length and Persistence Length of Xanthan in Solutions with Different Salt Concentrations

	contour length			
	number average L_n (nm)	weight average L_w (nm)	polydispersity index L_w/L_n	persistence length L_p (nm)[a]
water	1651	1922	1.16	417
0.01 M KCl	824	1170	1.42	370
0.1 M KCl	575	738	1.28	141
0.5 M KCl	450	603	1.34	168

[a] Persistence length calculation based on eq 2. Measured values were significantly different at $P = 0.05$ (one-way ANOVA, Student *t*-test).

Results

Conformational Changes as a Function of Ionic Strength. The contour length of the polymer was greatest when no salt was present and decreased as the salt concentration increased (Table 1). In pure water, the number and weighted average contour lengths were 1651 and 1922 nm, respectively, while these values were 450 and 603 nm in 0.5 M KCl. The polydispersity of the sample gives rise to the differences in the number and weight-averaged contour lengths (Table 1). The distributions of contour lengths at each salt concentration are shown in the corresponding histograms (Figure 1). Each treatment caused a statistically significant change in the contour length, based on a Student's *t*-test.

We must note that the resolution of the images varied depending on the scan size. Xanthan molecules in salt were captured as 4×4 μm scans at 512 lines per scan, to maximize the resolution achievable (resolution of ~8 nm). However, the xanthan chains in the absence of salt had to be imaged at larger scan sizes, as high as 8×8 μm (for a resolution of ~16 nm). We determined that a 50% zoom on an image caused less than a 1% change in the calculated contour length for an 800 nm chain. While the error may be slightly higher for short chains, all of our chain lengths are rather long, and so error from this source is not important.

Persistence Length Calculation. The persistence length was calculated for xanthan chains in each of the four solutions. According to eq 3, the inverse slope of a plot of $\langle\theta^2\rangle$ vs l is equal to L_p. Values for l were chosen up to ~85−90% of the total contour length, and L_p values were calculated (Figure 2). Although the intercept of the best-fit lines is not zero, Frontali et al.[24] explained that this offset is the result of a small amount of experimental error. This error may result from the resolution limitations.

To check if the distribution of the bend angles was Gaussian, eq 4 was used. Plots of $\langle\theta^4\rangle/\langle\theta^2\rangle^2$ should yield values equal to 3. While our values approached 3, some deviation was seen, especially at large l values (Figure 3). Rivetti et al.[25] also observed deviations from Gaussian behavior in their analysis of DNA conformation at both ends of the chain and attributed these deviations to the finite pixel size of the images.

Flexibility of Xanthan Chains. The rigidity of the polymer generally decreased as salt was added (Table 1). Xanthan in pure water had the highest persistence length (417 nm), and the persistence length decreased to 370 nm when some salt was present in solution (0.01 M KCl). L_p decreased to ~140−170 nm in 0.1 and 0.5 M KCl.

Upon going from no salt to 0.01 M KCl, the change in polymer flexibility was observed from the AFM images.

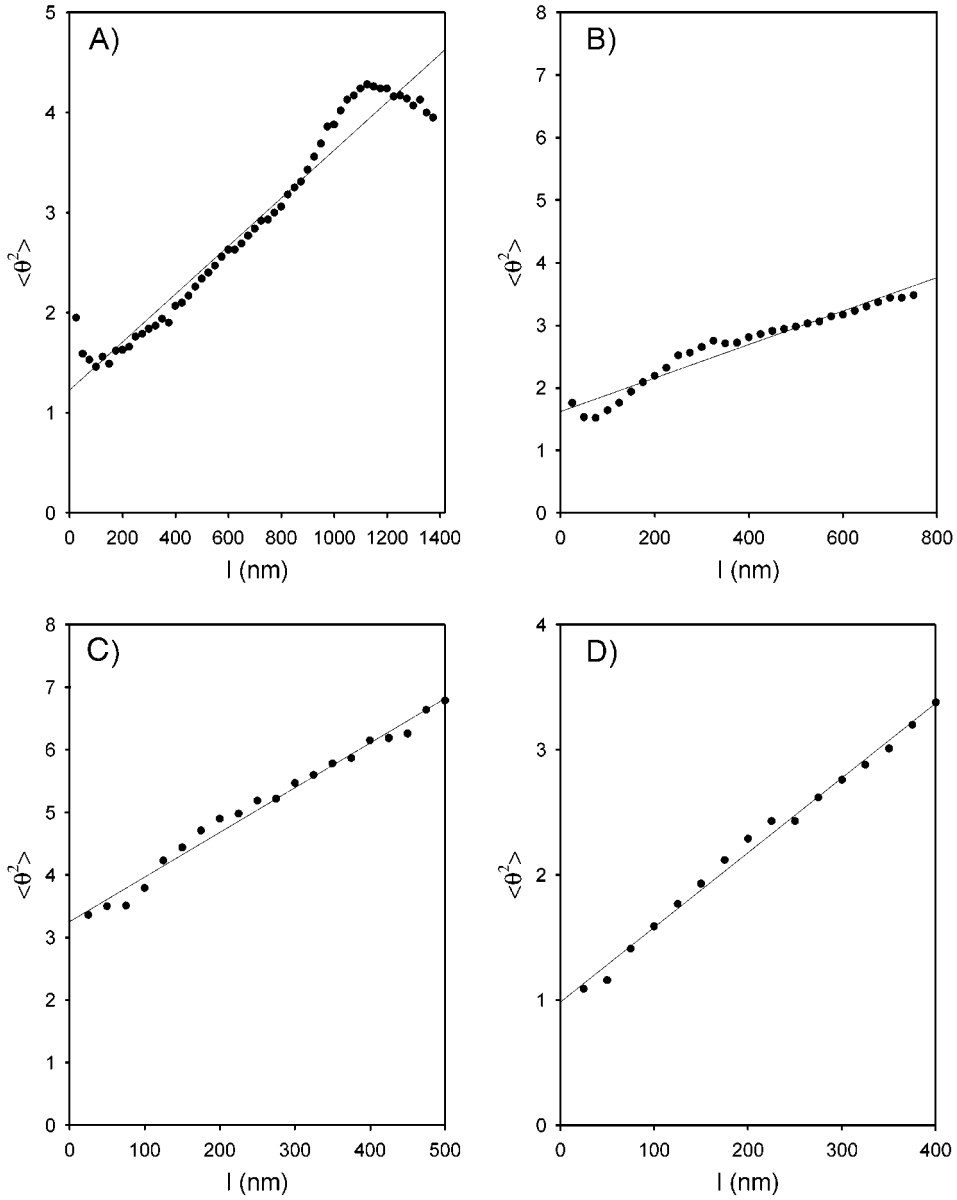

Figure 2. $\langle\theta^2\rangle$ vs the contour distance, *l*, for (A) pure water, (B) 0.01 M KCl, (C) 0.1 M KCl, and (D) 0.5 M KCl. Linear regression lines are shown.

While xanthan in pure water appeared elongated (Figure 4), coiling or bending of the molecule appeared to occur (Figure 5) when some salt was present. This trend continued as the salt concentration increased, with the xanthan molecules in 0.1 and 0.5 M KCl being the most flexible (Figure 6). As shown in Figure 6, a tendency toward aggregated molecules was observed when 0.1 M KCl was also present, although only individual molecules were included in the image analysis.

Thermal-induced Denaturation and Renaturation. Heating causes the xanthan helix to break apart,[7] but it can be reformed if salt is present. For xanthan in pure water, the double helix did not fully reform (Figure 7). Several pieces of evidence point to xanthan being present in a single helical structure in pure water and a double helical structure in salt solution. First, the single helical structure could sometimes be observed as the presence of thin regions and loops in the images. For example, the thickness of the single helix portion of the chain, indicated by the arrow in Figure 7A, is almost twice the thickness of the double chain region, indicated in Figure 7B (0.86 and 0.48 nm, respectively). For xanthan molecules in pure water, loops were observed in 23% of the images (Figure 7C), and thin regions were observed in 53%. These phenomena were never observed when salt was present. Second, the contour length decreased by about half upon going from pure water to 0.01 M KCl. These length changes support the explanation that the xanthan chains undergo a transformation from a single to double helical structure when salt is added.

Role of Mica Substrate on Conformation. Calculations of the predicted 2D and projected conformations allowed for the determination of whether the measured end-to-end distance was an equilibrium measurement or if the molecules were trapped in a nonequilibrium conformation on the surface. The large standard deviations for the end-to-end distances (Table 2) should be interpreted cautiously. The values do not represent "error", but rather, are in large part due to the polydispersity inherently present in the chains

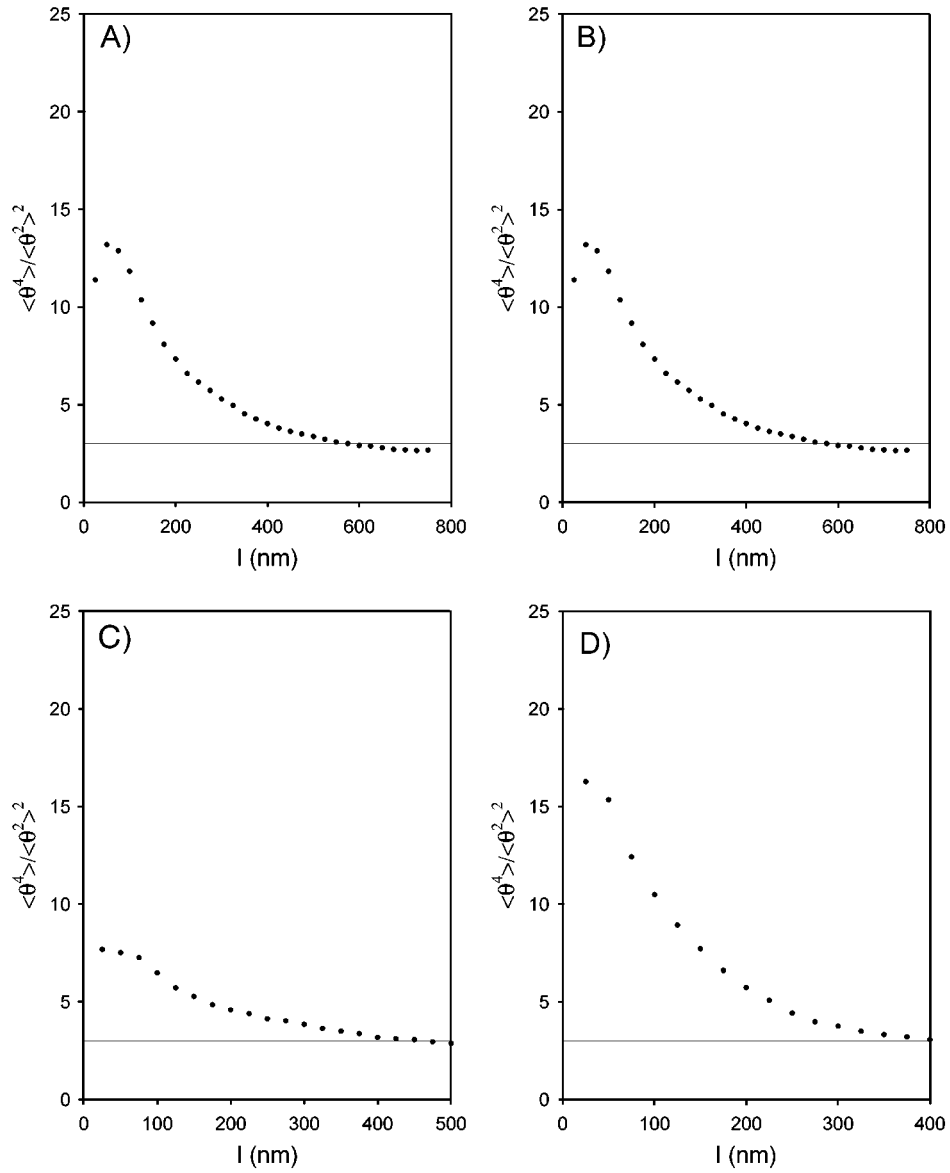

Figure 3. $\langle\theta^4\rangle/\langle\theta^2\rangle^2$ vs the contour distance, *l*, for (A) pure water, (B) 0.01 M KCl, (C) 0.1 M KCl, and (D) 0.5 M KCl. The horizontal line in each graph represents $\langle\theta^4\rangle/\langle\theta^2\rangle^2$ equal to 3.

Table 2. Measured and Calculated End-to-End Distances for Xanthan Chains

	measured $\langle R_{ee}\rangle^a$ (nm)	calculated $\langle R_{ee}\rangle_{2D}$ (based on L_n) (nm)	calculated $\langle R_{ee}\rangle_{proj}$ (based on L_n) (nm)
water	1168 ± 472	1247	831
0.01 M KCl	541 ± 329	696	494
0.1 M KCl	390 ± 224	431	286
0.5 M KCl	328 ± 172	368	256

[a] Measured values were significantly different at $P < 0.05$ (one-way ANOVA, Student's *t*-test).

(Table 1). Despite the polydispersity, all of the calculations based on a projected conformation under-predicted the measured values, which were systematically closer to the values calculated based on a 2D conformation on the surface.

Discussion

The secondary structure of xanthan has been the subject of much study, in part due to xanthan's widespread uses,

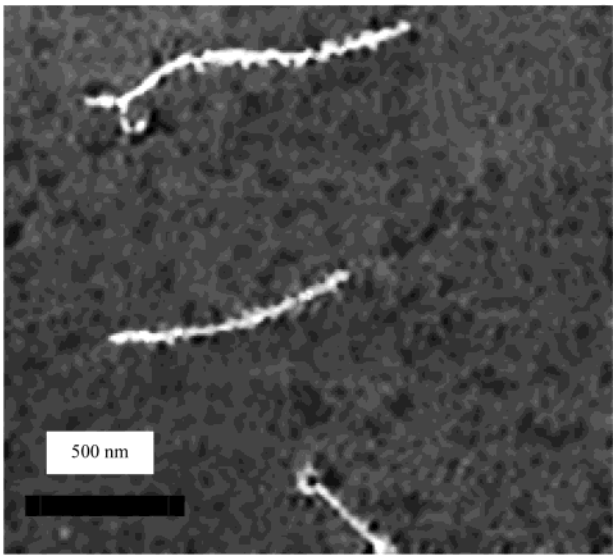

Figure 4. Representative image of xanthan in pure water, allowed to adsorb onto mica for 1 min.

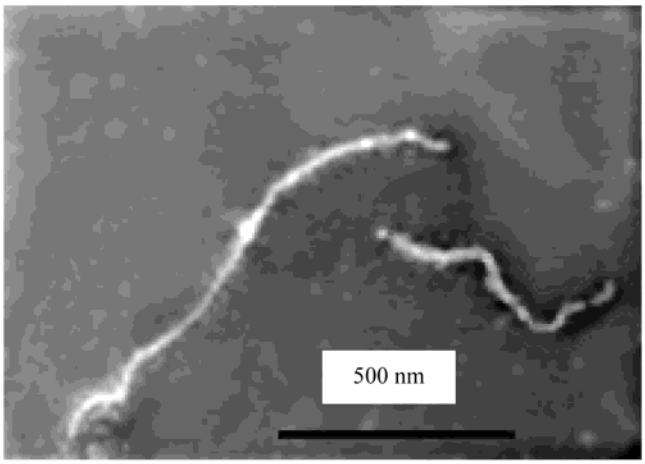

Figure 5. Representative image of xanthan from 0.01 M KCl solution, allowed to adsorb onto mica for 1 min.

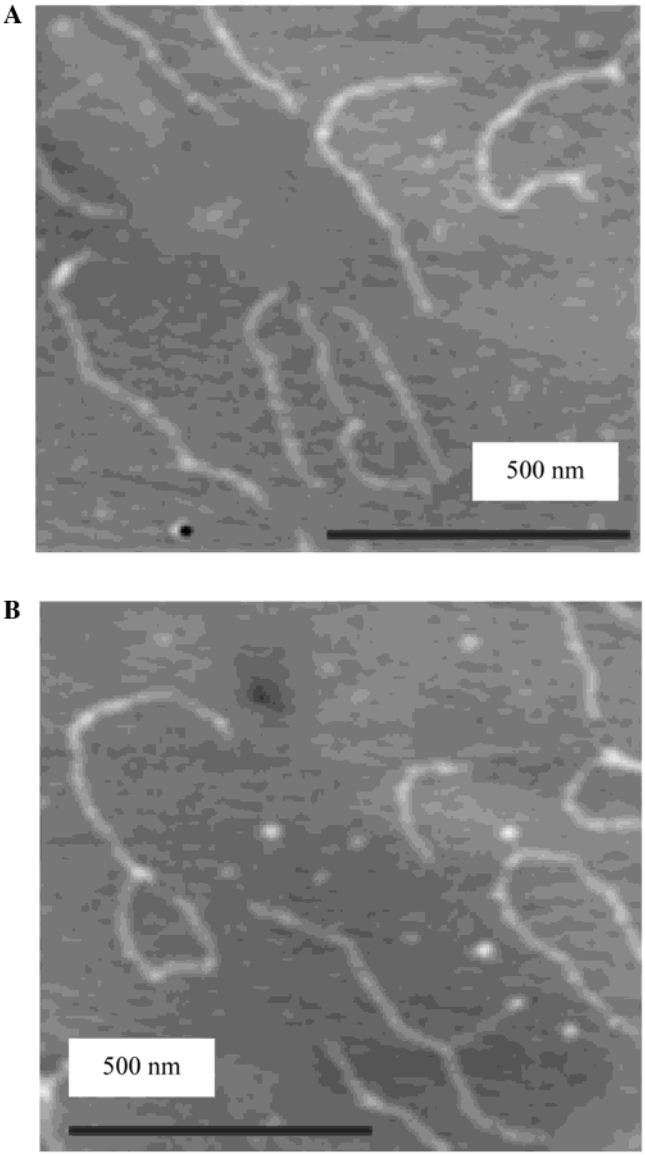

Figure 6. Representative images of xanthan chains in (A) 0.1 M KCl and (B) 0.5 M KCl, allowed to adsorb onto mica for 1 min.

and in part due to the controversy surrounding its conformation. Although AFM imaging and force measurements of xanthan have been performed previously,[21,22,27−29] this study is the first to quantitatively analyze the changes in xanthan's conformation as a function of salt concentration using single-molecule AFM imaging.

Temperature and Ionic Strength Induced Changes in Xanthan Conformations. The temperature and ionic strength induced transitions in xanthan from an ordered to disordered structure are well documented,[6−8] but the secondary structure is still a subject of debate. Native xanthan is generally believed to exist in a double helical state[7,11,13,23] that can be denatured through exposure to high temperature or very low ionic strength.

Along with the debate over the ordered conformation of xanthan, there has been a debate over how the conformation changes upon heating, and whether it is reversible. Kawakami et al.[30] demonstrated from viscosity, optical rotation, and sedimentation equilibrium measurements that at least 70% of xanthan dimers dissociate into monomers when heated to 95 °C for 9 h. The denatured conformation is that of a single helix. Xanthan can also be renatured if it is gradually cooled after heating above the conformational melting temperature. However, the denaturation is reversible only if sufficient salt is present.[2]

We did not examine native xanthan. Therefore, we cannot comment on the percentage of molecules that dissociate upon exposure to heat or whether the renatured form is identical to the native form. These subjects have been debated elsewhere.[2,11,31,32] However, we did observe that renaturation was dependent on salt concentration. Xanthan was renatured when salt was present. When salt was not present, renaturation was incomplete, as could be observed by loops or thin regions in the images and the doubling of the contour length.

The contour length changed drastically in going from pure water to salt solution. We speculate that this change is due to differences in the helical structure of the xanthan molecules. In salt solution, xanthan forms a double helix, while when no salt was present, the molecules were present in a single helical state. Nonetheless, this change could not be verified by height measurements. The height of the molecules was the same in pure water and 0.5 M KCl (∼0.85 nm). The xanthan molecules may have been more compressed in water, but unfortunately, under conditions of drastically varying ionic strength, AFM cannot be used to accurately measure the thicknesses of the molecules. Furthermore, horizontal distances cannot be measured accurately because the probe geometry will broaden these measurements substantially.

Subsequent changes in the contour length upon adding more salt seem to reflect a reduction in intramolecular repulsive interactions. When low or no salt was present, intramolecular electrostatic repulsion was strong. Both the backbone and the side chains of xanthan possess a negative charge. The molecule stretches to minimize repulsive intramolecular interactions. The presence of salt diminished this repulsion, and allowed for more bending to occur. Thus, the persistence length decreased when salt was present.

Intermolecular repulsion also decreased at higher salt concentrations. Although this effect was not quantified, associated molecules (in pairs or aggregates) were observed only in the presence of $\geq$0.1 M KCl.

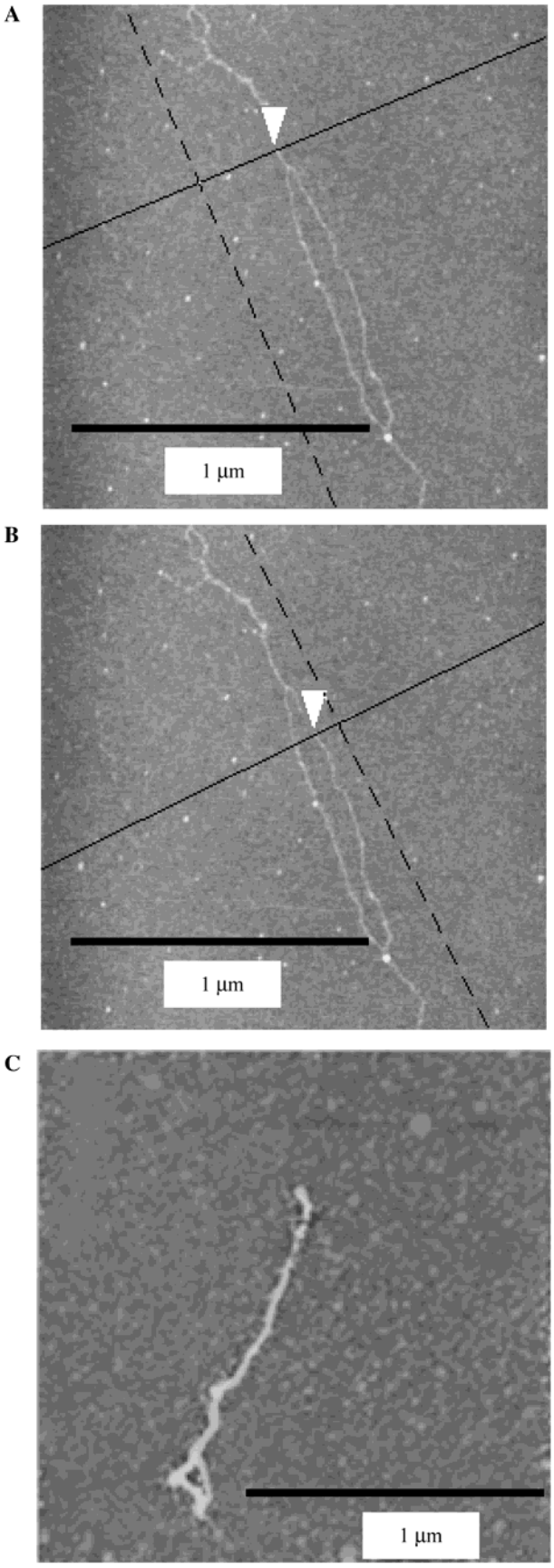

Figure 7. Incomplete renaturation of xanthan chain in pure water. (A) Where renaturation has occurred, there is a double helix with a height of 0.86 nm. (B) Where renaturation has not occurred, there is a single helix with a height of 0.48 nm. (C) Another example is shown of incomplete renaturation of xanthan in pure water. Arrows point to regions where strands are very thin or a loop has formed.

Persistence Length. Our studies suggest that renatured xanthan has a persistence length between 141 and 417 nm, depending on salt concentration. Direct imaging (electron micrographs) by Stokke et al.[25] yielded L_p values of 150 nm for double stranded xanthan (in 0.1 M ammonium acetate) and 60 nm for single stranded xanthan (in 2 mM ammonium acetate). Note that these samples were not heated, but the presence of single or double helices was attributed to the presence/absence of salt.

Solution techniques have been used with varying results in calculating the persistence length of native and denatured xanthan, with values generally ranging from 30 to 130 nm. The persistence length of (native) xanthan was estimated to be 50 nm in 0.086 M NaCl, based on viscosity measurements and the assumption that the wormlike chain (WLC) model is valid.[18] Milas and Rinaudo[33] estimated persistence lengths of 29−40 nm for native xanthan, and 41−73 nm for denatured xanthan, based on light scattering and viscosity measurements. Their calculations were also based on wormlike chain behavior. Sato et al.[17,34] measured persistence lengths of 100−130 nm for native xanthan in 0.1 M NaCl, based on light scattering, sedimentation, and viscosity measurements.

The range of values reported in the literature reflects, in large part, different preparation techniques and different sampling conditions and, in some cases, the model assumptions. The advantage of calculating polymer conformation from AFM imaging is that the artifacts associated with solution techniques (aggregate formation, in particular) are eliminated and it is not necessary to invoke WLC assumptions. Also, deviations from the average behavior can be observed. For example, only an imaging technique could demonstrate the incompletely reformed helix and loop structures shown in Figure 7.

In comparison with other polysaccharide biopolymers, xanthan is quite rigid. Succinoglycan, for example, has a persistence length between 36 and 105 nm in 0.01 M KCl and water, respectively.[34] Paradossi and Brant[13] suggested that interactions between the trisaccharide side chains and backbone might cause a greater conformational constraint in xanthan as compared to other highly substituted cellulosics. The rigidity of xanthan and the high conformational transition temperature at salt concentrations commonly encountered in industrial applications have given rise to xanthan's commercially viable properties.

Single-molecule AFM imaging has great potential to complement existing information on biopolymer conformation available from solution studies. Although, in this study, a direct comparison between AFM and solution measurements was not possible due to the various preparation techniques used in the literature, theoretical calculations have helped us to conclude that the AFM technique can yield reliable results that are representative of solution conformations. The calculation of the end-to-end distances of the xanthan chains and comparisons with the measured values (Table 2) confirmed that the conformations we observed were equilibrium conformations (i.e., the same as what would be observed in solution). Previous work with DNA, for which much more experimental data is available, was helpful in

proving that these calculations can be used to distinguish between equilibrium and nonequilibrium conformations of biopolymers.[26] However, as with any microscopic technique, most structural modifications are introduced during the highly critical sample preparation step. Great care is required if AFM observations are to be representative of solution conformations.

Implications

This study provided new direct evidence in support of the double helical conformation of xanthan, and for the reversibility of the thermal denaturation/renaturation when sufficient salt was present. This single-molecule microscopy technique can be applied to other systems in order to gain new insight into the conformation behavior of many other biopolymers. Our future work involves applying these techniques to microbial polymers that are known to be important in environmental or colloidal applications.

Acknowledgment. T.A.C. would like to thank the CABE group for hosting her during this project, especially Jacques Buffle, Denis Mavrocordatos, Françoise Meunier, Serge Stoll, and Lahoussine Ouali for their helpful discussions and experimental assistance. Thanks to Nehal Abu-Lail for proofreading this manuscript. This work was supported by Swiss National Funds 2000-061648.001 and 2000-050629.971.

References and Notes

(1) Rijnaarts, H. H. M.; Norde, W.; Lyklema, J.; Zehnder, A. J. B. *Colloids Surf. B: Biointerfaces* **1995**, *4*, 191.
(2) Jucker, B. A.; Zehnder, A. J. B.; Harms, H. *Environ. Sci. Technol*. **1998**, *32*, 2909.
(3) Corpe, W. A. In *Developments in Industrial Microbiology*; Murray, E. D., Bourguin, A. W., Eds.; Brown Publishers: Dubuque, IA, 1974; Vol. 15, p 281.
(4) Wilkinson, K. J.; Balnois, E.; Leppard, G. G.; Buffle, J. *Colloids Surf. A: Physicochem. Eng. Asp*. **1999**, *155*, 287.
(5) Jeanes, A.; Pittsley, J. E.; Senti, F. R. *J. Appl. Polym. Sci*. **1961**, *5*, 519.
(6) Holzwarth, G. *Biochemistry* **1976**, *15*, 4333.
(7) Holzwarth, G.; Prestridge, E. B. *Science* **1977**, *197*, 757.
(8) Morris, V. J.; Franklin, D.; I'Anson, K. *Carbohydr. Res.* **1983**, *121*, 13.
(9) Morris, E. R.; Rees, D. A.; Young, G.; Walkinshaw, M. D.; Darke, A. *J. Mol. Biol.* **1977**, *110*, 1.
(10) Milas, M.; Rinaudo, M.; Duplessix, R.; Borsali, R.; Lindner, P. *Macromolecules* **1995**, *28*, 3119.
(11) Capron, I.; Brigand, G.; Muller, G. *Polymer* **1997**, *38*, 5289.
(12) Norton, I. T.; Goodall, D. M.; Frangou, S. A.; Morris, E. R.; Rees, D. A. *J. Mol. Biol.* **1984**, *175*, 371.
(13) Paradossi, G.; Brant, D. A. *Macromolecules* **1982**, *15*, 874.
(14) Gamini, A.; Mandel, M. *Biopolymers* **1994**, *34*, 783.
(15) Rodd, A. B.; Dunstan, D. E.; Boger, D. V. *Carbohydr. Polym*. **2000**, *42*, 159.
(16) Kitamura, S.; Takeo, K.; Kuge, T.; Stokke, B. T. *Biopolymers* **1991**, *31*, 1243.
(17) Sato, T.; Norisuye, T.; Fujita, H. *Macromolecules* **1984**, *17*, 2696.
(18) Muller, G.; Lecourtier, J.; Chauveteau, G.; Allain, C. *Makromol. Chem., Rapid Commun*. **1984**, *5*, 203.
(19) Besio, G. J.; Leavesley, I. M.; Robert, K. *J. Appl. Polym. Sci*. **1987**, *33*, 825.
(20) Gamini, A.; de Bleijser, J.; Leyte, J. C. *Carbohydr. Res.* **1991**, *220*, 33.
(21) Kirby, A. R.; Gunning, A. P.; Morris, V. J. *Carbohydr. Res.* **1995**, *267*, 161.
(22) Gunning, A. P.; Kirby, A. R.; Morris, V. J. *Ultramicroscopy* **1996**, *63*, 1.
(23) Capron, I.; Alexandre, S.; Muller, G. *Polymer* **1998**, *39*, 5725.
(24) Frontali, C.; Dore, E.; Ferrauto, A.; Gratton, E. *Biopolymers* **1979**, *18*, 1353.
(25) Stokke, B. T.; Elgsaeter, A.; Skjak-Braek, G.; Smidsrod, O. *Carbohydr. Res*. **1987**, *160*, 13.
(26) Rivetti, C.; Guthold, M.; Bustamante, C. *J. Mol. Biol*. **1996**, *264*, 919.
(27) Rief, M.; Fernandez, J. M.; Gaub, H. E. *Phys. Rev. Lett.* **1998**, *81*, 4764.
(28) Li, H.; Rief, M.; Oesterhelt, F.; Gaub, H. E. *Appl. Phys. A.* **1999**, *68*, 407.
(29) Li, H.; Rief, M.; Oesterhelt, F.; Gaub, H. E. *Adv. Mater.* **1998**, *4*, 316.
(30) Kawakami, K.; Okabe, Y.; Norisuye, T. *Carbohydr. Polym*. **1991**, *14*, 189.
(31) Capron, I.; Brigand, G.; Muller, G. *Int. J. Biomol.* **1998**, *23*, 215.
(32) Milas, M.; Reed, W. F.; Printz, S. *Int. J. Biol. Macromol*. **1996**, *18*, 211.
(33) Milas, M.; Rinaudo, M. *Carbohydr. Res.* **1986**, *158*, 191.
(34) Sato, T.; Kojita, S.; Noritsuye, T.; Fugita, H. *Polym. J.* **1984**, *16*, 423.
(35) Balnois, E.; Stoll, S.; Wilkinson, K. J.; Buffle, J.; Rinaudo, M.; Milas, M. *Macromolecules* **2000**, *33*, 7440.

BM015555G